From gymnastics to virtual nonholonomic constraints: energy injection, dissipation, and regulation for the acrobot

Adan Moran-MacDonald, *Member, IEEE*, Manfredi Maggiore, *Member, IEEE**, and Xingbo Wang

***Abstract*— In this article we study virtual nonholonomic constraints, which are relations between the generalized coordinates and generalized momenta of a mechanical system that can be enforced via feedback control. We design a constraint which emulates gymnastics giant motion in an acrobot, and rigorously prove that this constraint will inject or dissipate energy. This constraint is tested in simulation and on a real-world acrobot, demonstrating highly effective energy regulation properties and robustness to a variety of disturbances.**

***Index Terms*— energy regulation, virtual nonholonomic constraints, acrobot, gymnastics.**

I. Introduction

In gymnastics terminology, a "giant" is the motion a gymnast performs to achieve full rotations around a horizontal bar [1]. A gymnast will begin by hanging at rest, then swing their legs appropriately to gain energy over time. The authors of [2] modelled the gymnast as a variable length pendulum, and studied how the pendulum's length changes as a function of the gymnast's limb angle. Labeling the pendulum length by r and the gymnast's body orientation by θ, they observed experimentally that the value $\dot{r}/r$ has the biggest impact on the magnitude of energy injection. After testing several gymnasts under a variety of experimental conditions, they discovered that the peak value of $\dot{r}/r$ occured at the same fixed value of $\dot{\theta}/\theta$ for all gymnasts. In other words, gymnasts appear to move their legs as a function of their body angle and velocity when performing giants; doing so allows them to gain energy and rotate around the bar.

While the simplest model of a gymnast is the variable-length pendulum, a more realistic model is the two-link acrobot (Figure 1). Here, the top link represents the torso while the bottom link represents the legs. The acrobot is actuated exclusively at the center joint (the hip). Controlling the acrobot is a nontrivial task because it is not feedback linearizable [3]. To solve the swingup problem, one might begin by designing a leg controller which provably injects energy into the acrobot, so that the resulting motion mimics that of a human performing a giant.

Manuscript submitted for review on September 9, 2021.

A. Moran-MacDonald (e-mail: adan.moran@mail.utoronto.ca) and M. Maggiore (e-mail: maggiore@control.utoronto.ca) are with the Department of Electrical and Computer Engineering, University of Toronto, ON, Canada.

X. Wang is with ??? (e-mail: ???).

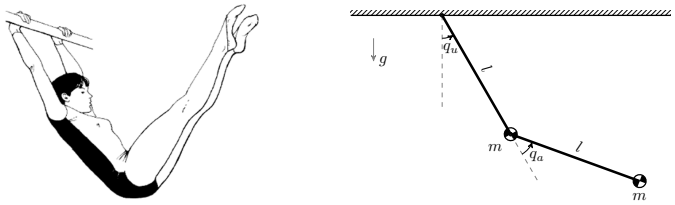

Fig. 1: A simplified two-link acrobot as a model for a gymnast. Image modified from [4].

Previous attempts at acrobot giant generation have involved trajectory tracking, partial feedback linearization, or other energy-based methods (see [5]–[8]). While all these approaches succeed at making the acrobot rotate around the bar, none of them use the results of [2]. That is, none of these leg controllers track a function of the acrobot's body angle and velocity. In 2016, Wang designed a controller [4] which tracked the body angle and an *estimate* of the velocity, but not the velocity itself. His approach was a preliminary version of a recent technique know as the method of virtual nonholonomic constraints [9].

Virtual nonholonomic constraints (VNHCs) have been used for human-robot interaction [10]–[12], error-reduction on time-delayed systems [13], and they have shown marked improvements to the field of bipedal locomotion [9], [14], [15]. Indeed, they produce more robust walking motion in biped robots than other virtual constraints which do not depend on velocity [16]. In particular, VNHCs may be capable of injecting and dissipating energy from a system in a robust manner, all while producing realistic biological motion.

In this article, we design a virtual nonholonomic constraint which provably injects energy into the acrobot through human-like giant motion. In particular, any acrobot constrained by this VNHC is guaranteed to perform rotations around the bar. Under suitable conditions on the acrobot's physical parameters, this VNHC also enables the acrobot to rotate around the bar at a desired speed. We will provide simulations to show how one can use VNHCs to regulate energy, along with experimental results which demonstrate the robustness of this behaviour to model uncertainty, sensor noise, and a variety of external disturbances.

Notation: We use the following notation and terminology in this article. The $n \times n$ identity matrix is denoted I_n, and the $n \times m$ matrix of zeros is denoted $\mathbf{0}_{n\times m}$. A matrix

$A \in \mathbb{R}^{n\times m}$ is *right semi-orthogonal* if $AA^\mathsf{T} = I_n$ and is *left semi-orthogonal* if $A^\mathsf{T}A = I_m$. For $A \in \mathbb{R}^{n\times m}$ and $B \in \mathbb{R}^{p\times m}$, we define $[A;B] \in \mathbb{R}^{(n+p)\times m}$ as the matrix obtained by stacking A on top of B. Given $\sigma_1, \ldots, \sigma_n \in \mathbb{R}$, we define $\operatorname{diag}(\sigma_1, \ldots, \sigma_n) \in \mathbb{R}^{n\times n}$ as the diagonal matrix whose value at row i, column i is σ_i. For $T > 0$, the set of real numbers modulo T is denoted $[\mathbb{R}]_T$, with $[\mathbb{R}]_\infty := \mathbb{R}$. The gradient of a matrix-valued function $A : \mathbb{R}^m \to \mathbb{R}^{n\times n}$ is the block matrix of stacked partial derivatives, $\nabla_x A := [\partial A/\partial x_1; \cdots; \partial A/\partial x_m] \in \mathbb{R}^{nm\times n}$. Given two matrices $A \in \mathbb{R}^{n\times m}$ and $B \in \mathbb{R}^{r\times s}$, the Kronecker product (see [17]) is the matrix $A \otimes B \in \mathbb{R}^{nr\times ms}$ defined as

$$A \otimes B = \begin{bmatrix} A_{1,1}B & \cdots & A_{1,m}B \\ \vdots & \ddots & \vdots \\ A_{n,1}B & \cdots & A_{n,m}B \end{bmatrix}. \tag{1}$$

The Poisson bracket [18] between the functions $f(q,p)$ and $g(q,p)$ is

$$[f,g] := \sum_{i=1}^{n} \frac{\partial f}{\partial p_i}\frac{\partial g}{\partial q_i} - \frac{\partial f}{\partial q_i}\frac{\partial g}{\partial p_i}. \tag{2}$$

The Kronecker delta δ_i^j is 1 if $i = j$ and 0 otherwise. Finally, we say a function $R(I)$ is $O(I^2)$ if $\lim_{I\to 0} R(I)/I = 0$.

II. Problem Formulation

We will use the simplified acrobot model in Figure 1, where we assume the torso and leg rods are of equal length l with equal point masses m at the tips. The acrobot's configuration is described in generalized coordinates (q_u, q_a) on the configuration manifold $\mathcal{Q} = \mathbb{S}^1 \times \mathbb{S}^1$, where q_u is unactuated and q_a is actuated. We ignore dissipative forces in this model.

The acrobot has inertia matrix M, potential function V (with respect to the horizontal bar), and input matrix B given as follows:

$$M(q) = \begin{bmatrix} ml^2(3 + 2\cos(q_a)) & ml^2(1 + \cos(q_a)) \\ ml^2(1 + \cos(q_a)) & ml^2 \end{bmatrix}, \tag{3}$$

$$V(q) = -mgl(2\cos(q_u) + \cos(q_u + q_a)), \tag{4}$$

$$B = [0; 1]. \tag{5}$$

For reasons that will become clear later in this article, we use Hamiltonian mechanics to derive the dynamics of the acrobot. For this we require the conjugate of momenta, $p = (p_u, p_a) = M(q)\dot{q}$. The dynamics of the acrobot in (q,p) coordinates are given in (6). For shorthand, we write $c_u := \cos(q_u)$, $c_a := \cos(q_a)$, and $c_{ua} := \cos(q_u + q_a)$; likewise, $s_u := \sin(q_u)$, $s_a := \sin(q_a)$, and $s_{ua} := \sin(q_u + q_a)$.

$$\mathcal{H}(q,p) = \frac{1}{2}p^\mathsf{T}M^{-1}(q)p - mgl(2c_u + c_{ua}), \tag{6}$$

$$\begin{cases} \dot{q} = M^{-1}(q)p, \\ \dot{p}_u = -mgl(2s_u + s_{ua}), \\ \dot{p}_a = -\frac{1}{2}p^\mathsf{T}\nabla_{q_a}M^{-1}(q)p - mgls_{ua} + \tau. \end{cases}$$

The control input is a force $\tau \in \mathbb{R}$ affecting only the dynamics of p_a, representing a torque acting on the hip joint. Let us now define what it means for a mechanical system to gain or lose energy.

Definition 1: Let $\mathcal{Q}$ be an n-dimensional smooth manifold. Let $f : \mathcal{Q} \to T\mathcal{Q}$ be a smooth vector field and let $D \subset \mathcal{Q}$ be open. The system described by $\dot{x} = f(x)$ *gains energy on* D if, for all compact sets $K \subset D$ and for almost every initial condition $x(0) \in K$, there exists $T > 0$ such that $x(t) \notin K$ for all $t > T$. The system *loses energy on* D if it gains energy in negative-time.

The definition above applies to vector fields that are a not necessarily Hamiltonian, and therefore might not have an associated notion of "energy". The terms "gain energy" and "lose energy" are to be interpreted loosely in this context. Our goal is to design a smooth function $f : \mathbb{S}^1 \times \mathbb{R}$ such that the relation $q_a = f(q_u, p_u)$ for system (6) can be enforced asymptotically via feedback control (in Section III we call this a regular virtual nonholonomic constraint). We will further require that the dynamics of the acrobot, when the relation holds, gain or lose energy on some set D in the sense of Definition 1. Note that any system satisfying Definition 1 can have unstable equilibria on D, but not limit cycles nor closed orbits.

III. Theory of VNHCs

Before embarking on our design problem, we must summarize the relevant theory of virtual nonholonomic constraints for a class of mechanical systems we call "simply actuated hamiltonian systems". The results we provide in Section III-B are not novel: they are a special case of the results in [9].

A. Simply Actuated Hamiltonian Systems

Take a mechanical system modelled with generalized coordinates $q = (q_1, \ldots, q_n)$ on a configuration manifold $\mathcal{Q} = [\mathbb{R}]_{T_1} \times \cdots \times [\mathbb{R}]_{T_n}$, where $T_i = 2\pi$ if q_i is an angle and $T_i = \infty$ if q_i is a displacement. The corresponding generalized velocities are $\dot{q} = (\dot{q}_1, \ldots, \dot{q}_n) \in \mathbb{R}^n$.

Suppose this system has Lagrangian $\mathcal{L}(q,\dot{q}) = 1/2\ \dot{q}^T D(q)\dot{q} - P(q)$, where the potential energy $P : \mathcal{Q} \to \mathbb{R}$ is smooth, and the inertia matrix $D : \mathcal{Q} \to \mathbb{R}^{n\times n}$ is smooth and positive definite for all $q \in \mathcal{Q}$. The *conjugate of momentum* to q is the vector $p := \partial\mathcal{L}/\partial\dot{q} = D(q)\dot{q} \in \mathbb{R}^n$. As per [18], the *Hamiltonian* of the system in (q,p) coordinates is

$$\mathcal{H}(q,p) = \frac{1}{2}p^\mathsf{T}D^{-1}(q)p + P(q), \tag{7}$$

with dynamics

$$\begin{cases} \dot{q} = \nabla_p\mathcal{H}, \\ \dot{p} = -\nabla_q\mathcal{H} + B(q)\tau, \end{cases} \tag{8}$$

where $\tau \in \mathbb{R}^k$ is a vector of generalized input forces and the input matrix $B : \mathcal{Q} \to \mathbb{R}^{n\times k}$ is full rank for all $q \in \mathcal{Q}$. If $k < n$, we say the system is *underactuated* with degree of underactuation $(n - k)$.

Using the matrix Kronecker product, it is easy to show that (8) expands to

$$\begin{cases} \dot{q} = D^{-1}(q)p, \\ \dot{p} = -\frac{1}{2}(I_n \otimes p^\mathsf{T})\nabla_q D^{-1}(q)p - \nabla_q P(q) + B(q)\tau. \end{cases}$$

Because τ is transformed by $B(q)$, it is not obvious how any particular input force τ_i affects the system. As a first step in addressing this problem, we make the following assumptions.

Assumption 1: The input matrix $B(q) \equiv B \in \mathbb{R}^{n\times k}$ is constant and has full rank $k < n$.

When $\mathcal{Q} = \mathbb{R}^n$, the above assumption allows us to define a canonical coordinate transformation of (7) which decouples the input forces. To define this transformation we will make use of the following lemma.

Lemma 1: Suppose Assumption 1 holds. Then there exists a nonsingular matrix $\hat{T} \in \mathbb{R}^{k\times k}$ so that the regular feedback transformation

$$\tau = \hat{T}\hat{\tau}$$

has a new input matrix $\hat{B}$ for $\hat{\tau}$ which is left semi-orthogonal.

Proof: Since B is constant and full rank, it has a singular value decomposition $B = U^{\mathsf{T}}\Sigma V$ where $\Sigma = [\mathrm{diag}\,(\sigma_1,\ldots,\sigma_k)\,;\mathbf{0}_{(n-k)\times k}]$, $\sigma_i > 0$, and $U \in R^{n\times n}$, $V \in \mathbb{R}^{k\times k}$ are unitary matrices [19]. Defining $T = \mathrm{diag}\,(1/\sigma_1,\ldots,1/\sigma_k)$ and assigning the regular feedback transformation $\tau = VT\hat{\tau}$ yields a new input matrix $\hat{B} = BVT$ for $\hat{\tau}$ such that $\hat{B}^{\mathsf{T}}\hat{B} = T^{\mathsf{T}}\Sigma^{\mathsf{T}}\Sigma T = I_k$. ∎

In light of Lemma 1 there is no loss of generality in assuming that the input matrix is left semi-orthogonal, which means that B^{T} is right semi-orthogonal. Now, let $\mathbf{B} := [B^{\perp}; B^{\mathsf{T}}]$ where $B^{\perp} \in \mathbb{R}^{(n-k)\times k}$ is a left annihilator of B, i.e., $B^{\perp}B = \mathbf{0}_{(n-k)\times k}$. Since B is constant, such a $B^{\perp}$ exists and $\mathbf{B}$ is invertible.

The following theorem requires that $\mathcal{Q} = \mathbb{R}^n$ so that the coordinate transformation is well defined.

Theorem 1: Take the Hamiltonian system (7) with configuration manifold $\mathcal{Q} = \mathbb{R}^n$ and suppose Assumption 1 holds. The coordinate transformation $\left(\tilde{q} = (\mathbf{B}^{\mathsf{T}})^{-1}q, \tilde{p} = \mathbf{B}p\right)$ is a canonical transformation and the resulting dynamics are given by

$$\mathcal{H}(\tilde{q},\tilde{p}) = \frac{1}{2}\tilde{p}^{\mathsf{T}}M^{-1}(\tilde{q})\tilde{p} + V(\tilde{q}), \tag{9}$$

$$\begin{cases} \dot{\tilde{q}} = M^{-1}(\tilde{q})\tilde{p}, \\ \dot{\tilde{p}} = -\frac{1}{2}(I_n \otimes \tilde{p}^{\mathsf{T}})\nabla_{\tilde{q}}M^{-1}(\tilde{q})\tilde{p} \\ \qquad\quad - \nabla_{\tilde{q}}V(\tilde{q}) + \begin{bmatrix}\mathbf{0}_{(n-k)\times k}\\ I_k\end{bmatrix}\tau, \end{cases}$$

where $M^{-1}(\tilde{q}) := (\mathbf{B}^{\mathsf{T}})^{-1}D^{-1}(\mathbf{B}^{\mathsf{T}}\tilde{q})\mathbf{B}^{-1}$ and $V(\tilde{q}) := P(\mathbf{B}^{\mathsf{T}}\tilde{q})$.

Proof: Since $\mathbf{B}$ is constant, this transformation satisfies $\partial\tilde{q}_i/\partial p_j = \partial\tilde{p}_i/\partial q_j = 0$ for all $i,j \in \{1,\ldots,n\}$. This implies the Poisson brackets $[\tilde{q}_i,\tilde{q}_j]$ and $[\tilde{p}_i,\tilde{p}_j]$ are both zero. Then, one can show that $[\tilde{p}_i,\tilde{q}_j] = (\mathbf{B}^{\mathsf{T}})^{-1}_i(\mathbf{B}^{\mathsf{T}})_j = \delta^j_i$. By (45.10) in [18], this is a canonical transformation and the new Hamiltonian is $\mathcal{H}(\mathbf{B}^{\mathsf{T}}\tilde{q},\mathbf{B}^{-1}\tilde{p})$. Finally, since $\dot{\tilde{p}} = \mathbf{B}\dot{p}$, the input matrix for the system in $(\tilde{q},\tilde{p})$ coordinates is $\mathbf{B}B = [\mathbf{0}_{(n-k)\times k}; I_k]$, which proves the theorem. ∎

We call the $(\tilde{q},\tilde{p})$ coordinates *simply actuated coordinates*, and we call any Hamiltonian system whose input matrix is $[\mathbf{0}_{(n-k)\times k}; I_k]$ a *simply actuated hamiltonian system*. The first $(n-k)$ configuration variables in $\tilde{q}$, labelled q_u, are the *unactuated coordinates*; the remaining k configuration variables, labelled q_a, are the *actuated coordinates*. The corresponding (p_u, p_a) in $\tilde{p}$ are the *unactuated* and *actuated momenta*, respectively.

In this article we focus on the acrobot which, despite having a configuration manifold which is not $\mathbb{R}^n$, is already a simply actuated Hamiltonian system.

B. Virtual Nonholonomic Constraints

Griffin and Grizzle [14] were the first to define relative degree two nonholonomic constraints which can be enforced through state feedback. Horn *et al.* later extended their results in [9] to derive the constrained dynamics for a certain class of mechanical systems. These researchers made use of the unactuated conjugate of momentum, but they developed their results in the Lagrangian framework. In particular, they focused on Lagrangian systems with degree of underactuation one. We will now present a special case of [9] for simply actuated hamiltonian systems, so that the theory we apply to the acrobot is provided in its clearest form. After we finish this summary we will clarify the relationship between our material and that of [9].

For the rest of this section we take the system of inquiry to be a Hamiltonian mechanical system in simply actuated coordinates, as in (9). For simplicity of notation, we relabel $(\tilde{q},\tilde{p})$ to (q,p).

Definition 2: A *virtual nonholonomic constraint* (VNHC) *of order* k is a relation $h(q,p) = 0$ where $h : \mathcal{Q}\times\mathbb{R}^n \to \mathbb{R}^k$ is C^2, $\mathrm{rank}\,([dh_q,\, dh_p]) = k$ for all $(q,p) \in h^{-1}(0)$, and there exists a feedback controller $\tau(q,p)$ rendering the *constraint manifold* Γ invariant, where

$$\Gamma = \{(q,p) \mid h(q,p) = 0, dh_q\dot{q} + dh_p\dot{p} = 0\}. \tag{10}$$

The constraint manifold is a $2(n-k)$-dimensional closed embedded submanifold of $\mathcal{Q}\times\mathbb{R}^n$. A VNHC thereby allows us to study a reduced-order model of the system: it reduces the original $2n$ differential equations to $2(n-k)$ equations. In particular, if $k = (n-1)$, the constraint manifold is *always* 2-dimensional and its dynamics can be displayed on a plane.

In order to enforce the constraint $h(q,p) = 0$, we want to asymptotically stabilize the set Γ. To see when this is possible, let us define the error output $e = h(q,p)$. If any component of e_i has relative degree 1, we may not be able to stabilize Γ: we can always guarantee $e_i \to 0$, but not necessarily $\dot{e}_i \to 0$. It is for this reason that we define the following special type of VNHC.

Definition 3: A VNHC $h(q,p) = 0$ of order k is *regular* if the output $e = h(q,p)$ is of relative degree $\{2,2.\ldots,2\}$ everywhere on the constraint manifold Γ.

The authors of [9], [14] observed that relations which use only the unactuated conjugate of momentum often have vector relative degree $\{2,\ldots,2\}$. Indeed, we shall now prove that regular constraints cannot depend on the actuated momentum.

To ease notation in the rest of this section, we use the following shorthand:

$$\mathcal{A}(q,p_u) := dh_q(q,p_u)M^{-1}(q), \tag{11}$$

$$\mathcal{M}(q,p) := (I_{n-k}\otimes p^{\mathsf{T}})\nabla_{q_u}M^{-1}(q). \tag{12}$$

Theorem 2: A relation $h(q,p) = 0$ for system (9) is a regular VNHC of order k if and only if $dh_{p_a} = \mathbf{0}_{k\times k}$ and the decoupling matrix

$$\left(\mathcal{A}(q,p_u) - dh_{p_u}\mathcal{M}(q,p)\right)\begin{bmatrix}\mathbf{0}_{(n-k)\times k}\\ I_k\end{bmatrix}, \tag{13}$$

is invertible everywhere on the constraint manifold Γ.

Proof: Let $e = h(q,p) \in \mathbb{R}^k$. If $dh_{p_a} \neq \mathbf{0}_{k\times k}$ for some $(q,p) \in \Gamma$, then τ appears in $\dot{e}$ and the VNHC is not of relative degree $\{2,\dots,2\}$. Suppose now that $dh_{p_a} = \mathbf{0}_{k\times k}$. Then $\dot{e} = \mathcal{A}(q,p_u)p - dh_{p_u}\left(1/2\ \mathcal{M}(q,p)p + \nabla_{q_u}V(q)\right)$. Taking one further derivative provides $\ddot{e} = (\star) - dh_{p_u}\left(1/2\ d/dt\left(\mathcal{M}(q,p)p\right)\right) + \mathcal{A}(q,p_u)[\mathbf{0}_{(n-k)\times k}; I_k]\tau$, where $(\star)$ is a continuous function of q and p. One can further show that $dh_{p_u}\left(1/2\ d/dt\ \left(\mathcal{M}(q,p)p\right)\right) = (\star) + dh_{p_u}\mathcal{M}(q,p)[\mathbf{0}_{(n-k)\times k}; I_k]\tau$. Hence,

$$\ddot{e} = (\star) + \left(\mathcal{A}(q,p_u) - dh_{p_u}\mathcal{M}(q,p)\right)\begin{bmatrix}\mathbf{0}_{(n-k)\times k}\\ I_k\end{bmatrix}\tau,$$

which we write as $\ddot{e} = E(q,p) + H(q,p)\tau$ for appropriate E and H. From the definition of regularity, the VNHC h is regular when e is of relative degree $\{2,\dots,2\}$, which is true if and only if the matrix premultiplying τ is nonsingular, and hence that H is invertible. This proves the theorem. ∎

Under additional mild conditions (see [20]), a regular VNHC of order k can be stabilized by the output-linearizing state-feedback controller

$$\tau(q,p) = -H^{-1}(q,p)\left(E(q,p) + k_p e + k_d \dot{e}\right), \tag{14}$$

where $k_p, k_d > 0$ are control parameters which can be tuned on the resulting error dynamices $\ddot{e} = -k_p e - k_d \dot{e}$.

In Section IV we will enforce a regular constraint on the acrobot of the form $h(q,p) = q_a - f(q_u,p_u)$, where the actuators track a function of the unactuated variables. Regular constraints of this form always meet the mild conditions from [20], and hence we can stabilize the constraint manifold using (14). Since q_a is constrained to be a function of the unactuated variables, intuition tells us the constrained dynamics should be parameterized by (q_u,p_u). Unfortunately, $\dot{q}_u$ depends on p_a, and for general systems one cannot solve explicitly for p_a in terms of (q_u,p_u) because the $\dot{p}$ dynamics contain the coupling term $(I_n \otimes p^\mathsf{T})\nabla_q M(q)p$. We now introduce an assumption which allows us to solve for p_a as a function of (q_u,p_u), which in turn allows us to explicitly solve for the constrained dynamics.

Assumption 2: The inertia matrix does not depend on the unactuated coordinates, i.e., $\nabla_{q_u}M(q) = \mathbf{0}_{n(n-k)\times n}$.

Theorem 3: Let $\mathcal{H}$ be a hamiltonian system in simply actuated form (9) satisfying Assumption 2. Let $h(q,p_u) = q_a - f(q_u,p_u)$ be a regular VNHC of order k with constraint manifold Γ. Then the constrained dynamics are given by

$$\left.\begin{aligned}\dot{q}_u &= \begin{bmatrix}I_{(n-k)} & \mathbf{0}_{(n-k)\times k}\end{bmatrix}M^{-1}(q)p\\ \dot{p}_u &= -\nabla_{q_u}V(q)\end{aligned}\right|_{\substack{q_a = f(q_u,p_u)\\ p_a = g(q_u,p_u)}}, \tag{15}$$

where

$$g(q_u,p_u) := \left(\mathcal{A}(q,p_u)\begin{bmatrix}\mathbf{0}_{(n-k)\times k}\\ I_k\end{bmatrix}\right)^{-1}\cdot\Big(dh_{p_u}\nabla_{q_u}V(q) - \mathcal{A}(q,p_u)\begin{bmatrix}I_{(n-k)}\\ \mathbf{0}_{k\times(n-k)}\end{bmatrix}p_u\Big)\Big|_{q_a = f(q_u,p_u)}. \tag{16}$$

Proof: Setting $e = h(q,p_u)$ and using Assumption 2, we find that $\dot{e} = \mathcal{A}(q,p_u)p - dh_{p_u}\nabla_{q_u}V(q)$. Notice that $\mathcal{A}(q,p_u)p = \mathcal{A}(q,p_u)[\mathbf{0}_{(n-k)\times k}; I_k]p_a + \mathcal{A}(q,p_u)[I_{n-k}; \mathbf{0}_{k\times(n-k)}]p_u$. Since $h(q,p_u)$ is regular, $\mathcal{A}(q,p_u)[\mathbf{0}_{(n-k)\times k}; I_k]$ is invertible. Taking $e = \dot{e} = 0$, solving for p_a, and setting $q_a = f(q_u,p_u)$ completes the proof. ∎

We conclude this section by formalizing the notion of energy injection/dissipation for VNHCs.

Definition 4: A regular VNHC $h(q,p_u) = q_a - f(q_u,p_u)$ with constraint manifold Γ *injects (dissipates) energy on* $D \subset \Gamma$ if the constrained dynamics gain (lose) energy everywhere on D according to Definition 1, except possibly on a set of measure zero.

Comparison with existing literature: Horn *et al.* provide the constrained dynamics for VNHCs in [16]. Their assumption **H2** is what we call regularity, and our requirement that one can solve for $q_a = f(q_u,p_u)$ on Γ implies their assumption **H3** holds true. The only real distinction between this section and their work is that our constrained dynamics are explicit functions of the Hamiltonian coordinates (q_u,p_u). In fact, one can show that the constrained dynamics (15) coincide with the constrained dynamics in [9, Eqn. (17)] when one chooses the special case $\theta_1 = q_u$ and $\theta_2 = p_u$. This explicit representation will be beneficial when we apply the theory of VNHCs to the acrobot.

IV. The Proposed Acrobot VNHC

Our goal in this article is to design a VNHC which injects energy into the acrobot by means of a giant-like motion. Recall that the acrobot in Figure 1 has dynamics given by (6), repeated here for convenience:

$$\begin{cases}\dot{q} = M^{-1}(q)p,\\ \dot{p}_u = -mgl\left(2s_u + s_{ua}\right),\\ \dot{p}_a = -\frac{1}{2}p^\mathsf{T}\nabla_{q_a}M^{-1}(q)p - mgls_{ua} + \tau.\end{cases}$$

Since the control input τ only affects the actuated momentum, the system above is already in simply actuated form. Its state space is $\mathcal{Q}\times\mathcal{P}$ where $\mathcal{Q} = \mathbb{S}^1\times\mathbb{S}^1$, and $\mathcal{P} = \mathbb{R}\times\mathbb{R}$. We can therefore apply the theory from Section III to design a VNHC of the form $q_a = f(q_u,p_u)$ (i.e., a VNHC $h(q,p_u) = q_a - f(q_u,p_u) = 0$). Since we need the VNHC to be regular, the following proposition will be useful.

Proposition 1: Any relation $q_a = f(p_u)$ with $f \in C^2\left(\mathbb{R};\mathbb{S}^1\right)$ is a regular VNHC of order 1 for the acrobot in (6).

Proof: The decoupling matrix (13) for the acrobot evaluates to $((1+c_a)\partial_{q_u}f(q_u,p_u) + (3+2c_a))/(ml^2(2-c_a^2))$. Since $\partial_{q_u}f = 0$, this matrix is strictly positive for all values of q_a, and hence is full rank 1 everywhere on the constraint manifold. ∎

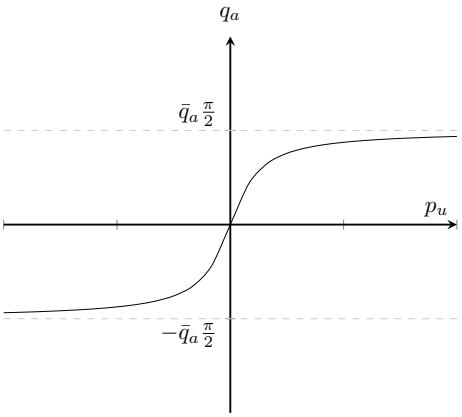

Fig. 2: The acrobot constraint $q_a = \bar{q}_a \arctan(Ip_u)$.

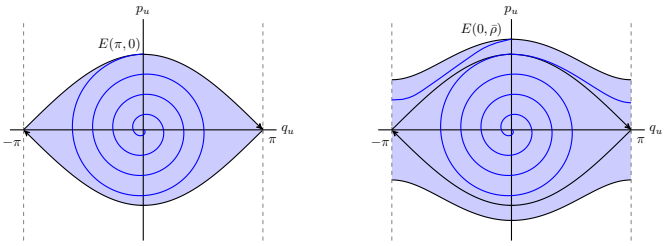

(a) The set $\mathcal{O}_1$. An orbit starting in this set (blue) will pass through the level set $E(\pi, 0)$ of the nominal pendulum.

(b) The set $\mathcal{O}_2(\rho)$. Orbits starting in this set are guaranteed to reach the level set $E(0, \rho)$ of the nominal pendulum.

Fig. 3: The sets on which the acrobot gains energy, according to Theorem 4.

To design our VNHC, we begin by examining a person on a seated swing. The person extends their legs when the swing moves forwards, and retracts their legs when the swing moves backwards. As the swing gains speed, the person leans their body while extending their legs higher, thereby shortening the distance from their center of mass to the pivot and adding more energy to the swing [21].

Now imagine the person's torso is affixed to the swing's rope so they are always upright. Imagine further that the swing has no seat, allowing the person to extend their legs beneath them. This position is identical to that of a gymnast on a bar.

The acrobot's legs are rigid rods which cannot retract, so we emulate the person on a swing by pivoting the legs toward the direction of motion. Since a person lifts their legs higher at faster speeds, the acrobot's legs should pivot to an angle proportional to the swing's speed. A real gymnast cannot swing their legs in full circles, though they are usually flexible enough to raise them parallel to the floor; hence, the VNHC must restrict the leg angle q_a to lie in $[-Q_a, Q_a]$ for some $Q_a \in [\frac{\pi}{2}, \pi[$. Because the direction of motion is entirely determined by p_u, one VNHC which emulates this process is $q_a = \bar{q}_a \arctan(Ip_u)$, displayed in Figure 2. Here, $\bar{q}_a \in]0, 2Q_a/\pi]$ and $I \in \mathbb{R}$ are design parameters.

This constraint does not perfectly recreate giant motion, during which the gymnast's legs are almost completely extended [1]. It instead pivots the legs partially during rotations. However, the behaviour is similar enough that this constraint will still inject energy into the acrobot. Our final VNHC is

$$h(q, p) = q_a - \bar{q}_a \arctan(Ip_u). \tag{17}$$

Recall that (q_u, p_u) denote the angle and momentum of the acrobot's torso. By Theorem 3, the constrained dynamics arising from the VNHC (17) are parameterized fully by $(q_u, p_u) \in \mathbb{S}^1 \times \mathbb{R}$. Here, (16) reduces to

$$g(q_u, p_u) = \frac{(1 + c_a)p_u}{ml^2(3 + 2c_a)} - \frac{mgl\bar{q}_a I(2 - c_a^2)(2s_u + s_{ua})}{(3 + 2c_a)(1 + I^2 p_u^2)},$$

and the constrained dynamics (15) are

$$\begin{cases} \dot{q}_u &= \frac{(1+I^2p_u^2)p_u + m^2gl^3\bar{q}_aI(2s_u+s_{ua})(1+c_a)}{ml^2(1+I^2p_u^2)(3+2c_a)}, \\ \dot{p}_u &= -mgl(2s_u + s_{ua}), \end{cases} \tag{18}$$

subject to $q_a = \bar{q}_a \arctan(Ip_u)$.

A. Energy Injection and Dissipation with the Proposed VNHC

Suppose for a moment that $I = 0$ in (17), i.e., that the legs stay fully extended. The acrobot becomes a nominal pendulum with two masses, whose total mechanical energy is

$$E(q_u, p_u) := \frac{p_u^2}{10ml^2} + 3mgl(1 - \cos(q_u)). \tag{19}$$

The upright equilibrium of this pendulum is located at $(q_u, p_u) = (\pi, 0)$. Imagine the pendulum hits the bottom of the swing arc with momentum $p_u \neq 0$. To reach the upright equilibrium, this momentum must be $p_u = \pm\sqrt{60m^2gl^3}$ because $E(\pi, 0) = E(0, \pm\sqrt{60m^2gl^3})$. If the momentum is smaller in magnitude, the acrobot will oscillate; if it is larger, the pendulum will rotate around the bar.

When the pendulum is oscillating, its state (q_u, p_u) lies in the set

$$\mathcal{O}_1 := \left\{(q_u, p_u) \in \mathbb{S}^1 \times \mathbb{R} \mid E(q_u, p_u) < E(\pi, 0)\right\}, \tag{20}$$

which is shown in Figure 3a. If for some $I \neq 0$ our VNHC injects energy into the acrobot on $\mathcal{O}_1$, and the constrained dynamics escape $\mathcal{O}_1$ and hit the vertical line $|q_u| = \pi$ in finite time, then the acrobot is guaranteed to perform giant-like motion and begin rotating around the bar.

When the pendulum is rotating with bounded momentum $|p_u| < \rho$ (for some chosen ρ), (q_u, p_u) must lie inside the rotation domain

$$\mathcal{R}(\rho) := \left\{(q_u, p_u) \in \mathbb{S}^1 \times \mathbb{R} \mid E(\pi, 0) < E(q_u, p_u) < E(0, \rho)\right\}. \tag{21}$$

Connecting the regions (20) and (21) yields the set

$$\mathcal{O}_2(\rho) := \left\{(q_u, p_u) \in \mathbb{S}^1 \times \mathbb{R} \mid E(q_u, p_u) < E(0, \rho)\right\}, \tag{22}$$

shown in Figure 3b. If the VNHC injects energy on $\mathcal{O}_2(\rho)$ for some $I \neq 0$, then the acrobot must necessarily swing up, begin rotating, and eventually rotate with a momentum of at least ρ.

Unfortunately, our VNHC does not always inject energy on $\mathcal{O}_1$ and $\mathcal{O}_2(\rho)$. If I is too large, the leg controller saturates and the body oscillates without gaining energy. However, choosing I small enough guarantees the legs will synchronize properly

with the body, and the acrobot will begin rotating around the bar. The following theorem provides conditions under which such an I exists.

Theorem 4: Consider the acrobot with Hamiltonian dynamics given in (6).

1) For each $m, g, l, \bar{q}_a > 0$, there exists $I^\star > 0$ such that, for all $I \in]0, I^\star]$, the VNHC (17) injects energy into the acrobot on $\mathcal{O}_1$. Moreover, every orbit of the constrained dynamics (18) will reach the line $|q_u| = \pi$ in finite time. If instead $I \in [-I^\star, 0[$, the VNHC dissipates energy on $\mathcal{O}_1$.
2) Let $C = m^2 g l^3 \bar{q}_a$ and define $b : \mathbb{S}^1 \times \mathbb{R}_{>0} \to \mathbb{R}$ by

$$b(\beta, \rho_0) := \frac{5C\left(\frac{C}{\bar{q}_a}\left(18 s_\beta^2 + 30 c_\beta(1 - c_\beta)\right) - c_\beta \rho_0^2\right)}{|\rho_0|\sqrt{\rho_0^2 - 30 m^2 g l^3 (1 - c_\beta)}}.$$

Define $S(\rho_0) := \int_0^{2\pi} b(\sigma, \rho_0) d\sigma$. Fix $\rho > \sqrt{60 m^2 g l^3}$ and suppose there exists $\epsilon > 0$ so that $S(\rho_0) \geq \epsilon$ for all $\rho_0 \in \left]\sqrt{60 m^2 g l^3}, \rho\right]$. Then there exists $I^{\star\star} \in]0, I^\star]$ such that, for all $I \in]0, I^{\star\star}]$, the VNHC (17) injects energy into the acrobot on $\mathcal{O}_2(\rho)$. If instead $I \in [-I^{\star\star}, 0[$, the VNHC dissipates energy on $\mathcal{O}_2(\rho)$.

Proof: See Section VII. ∎

Notice that $\mathcal{O}_1 \subset \mathcal{O}_2(\rho)$, yet Theorem 4 considers these sets separately. This separation is advantageous because the first result holds for any positive m, g, l, and $\bar{q}_a$. In other words, the first result of Theorem 4 states that all acrobots constrained by (17) will gain enough energy to begin rotating around the bar.

For the acrobot to achieve giants with energy $E(0, \rho)$, it must satisfy the assumption on the integral of $b(\beta, \rho_0)$. The value of this integral depends on the acrobot's physical parameters. If the assumption holds, there is some control value I (which depends on ρ) for which the acrobot will achieve rotations with a momentum of at least ρ.

B. Energy Regulation

One can apply the results of Theorem 4 towards energy regulation; that is, one can stabilize oscillations or rotations by appropriately toggling between injection and dissipation VNHCs, which can be achieved by changing the sign of I in (17). The acrobot is *oscillating* when it swings back and forth without performing a full revolution around the pivot point. Oscillations correspond to p_u changing sign periodically, and the peak torso angle (i.e., the point where an orbit crosses the q_u-axis) is called the *oscillation angle*. Conversely, the acrobot is *rotating* when its torso is performing full revolutions around the pivot, which corresponds mathematically to p_u maintaining the same sign. The momentum achieved by the acrobot at the bottom of the swing (i.e., the point where an orbit of rotation crosses the p_u-axis) is called the *rotation rate*.

Rotation Regulation: one chooses a desired rotation rate $p_{\text{des}} > 0$ and a hysteresis value $\delta \in [0, 1]$. Each time the orbit crosses the p_u-axis (i.e. when $q_u = 0$), the supervisor changes which VNHC is enforced as follows:

- If $|p_u| < (1 - \delta) p_{\text{des}}$, enable the injection VNHC by setting $I > 0$ in (17).
- If $|p_u| > (1 + \delta) p_{\text{des}}$, enable the dissipation VNHC by replacing $I > 0$ with $-I < 0$ in (17).
- If $(1 - \delta) p_{\text{des}} \leq |p_u| \leq (1 + \delta) p_{\text{des}}$, extend the leg fully by setting $q_a = 0$. In simulation we assume this can be done instantaneously, though in practice this takes time.

All orbits of the acrobot must cross the p_u axis, so this method will stabilize a rotation even if the acrobot is initialized in $\mathcal{O}_1$. While the above supervisor is designed to regulate a rotation rate, it cannot regulate the rotation direction.

The term "rotation regulation" implies that one must choose p_{des} and δ so that $(1-\delta)p_{\text{des}} > \sqrt{60 m^2 g l^3}$. In fact, it is entirely possible to choose p_{des} and δ so that $(1+\delta)p_{\text{des}} \leq \sqrt{60 m^2 g l^3}$. Rather than stabilizing a rotation, the supervisor would then stabilize an oscillation whose momentum at the bottom of the swing arc is p_{des}. However, there is a preferred method for stabilizing oscillations which we outline next.

Oscillation Regulation: one chooses a desired oscillation angle $q_{\text{des}} \in]0, \pi[$ and, to avoid infinite switching, a hysteresis value $\delta \in [0, \pi/q_{\text{des}} - 1]$. An orbit in the (q_u, p_u)-plane will either cross the q_u axis if the orbit corresponds to a rocking motion, or it will cross the line $|q_u| = \pi$ if the orbit corresponds to a full revolution. When either of these occur, the supervisor does the following:

- If $|q_u| < (1 - \delta) q_{\text{des}}$, enable the injection VNHC.
- If $|q_u| > (1 + \delta) q_{\text{des}}$, enable the dissipation VNHC.
- If $(1 - \delta) q_{\text{des}} \leq |q_u| \leq (1 + \delta) q_{\text{des}}$, keep the leg extended at $q_a = 0$. This can be done continously since $q_a = 0$ when $p_u = 0$.

Note that by our choice of δ, if the supervisor kicks in when $|q_u| = \pi$ (i.e., when the robot is rotating) then the supervisor will automatically enable the dissipation VNHC.

V. Simulation Results

In Section VI we will test our VNHC on a physical acrobot. This acrobot cannot be modelled by the simplified setup in Figure 1, because the torso and leg links have distributed mass. We must therefore use the more general acrobot model in Figure 4 to represent this system. Let us define

$$\begin{aligned} m_{11}(q) :=& m_a l_u^2 + 2 m_a l_u l_{c_a} \cos(q_a) + m_a l_{c_a}^2 + m_u l_{c_u}^2 \\ &+ J_u + J_a, \\ m_{12}(q) :=& m_a l_{c_a}^2 + m_a l_u l_{c_a} \cos(q_a) + J_a, \\ m_{22}(q) :=& m_a l_{c_a}^2 + J_a, \end{aligned}$$

where J_u and J_a are the moments of inertia of the torso and leg links respectively. The general acrobot has inertia matrix

$$M(q) = \begin{bmatrix} m_{11}(q) & m_{12}(q) \\ m_{12}(q) & m_{22}(q) \end{bmatrix},$$

and potential function

$$V(q) = g\big(m_a l_{c_a}(1 - c_{ua}) + (m_a l_u + m_u l_{c_u})(1 - c_u)\big).$$

Recall that we defined the sets $\mathcal{O}_1$ and $\mathcal{O}_2(\rho)$ used in Theorem 4 via the mechanical energy (19) of the nominal pendulum associated with a simplified acrobot. We obtained

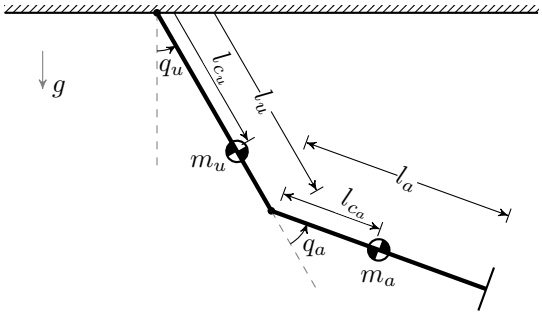

Fig. 4: The general acrobot model, represented by two weighted rods differing in both length and mass.

TABLE I: Physical parameters for the real acrobot.

m_u (kg)	m_a (kg)	l_u (m)	l_a (m)	l_{c_u} (m)	l_{c_a} (m)	J_u (kg·m^2)	J_a (kg·m^2)	g (m/s^2)
0.2112	0.1979	0.148	0.145	0.073	0.083	0.00129	0.00075	9.81

this nominal pendulum by setting $I = 0$ in (17). The boundary between oscillations and rotations of the nominal pendulum is obtained by finding the level set E_π of the nominal energy corresponding to the upright equilibrium $(q_u, p_u) = (\pi, 0)$.

We can extend this idea to find the nominal pendulum associated with our physical acrobot, whose parameters are provided in Table I. Setting $I = 0$ in (17) for this acrobot yields the mechanical energy of the nominal pendulum:

$$E(q_u, p_u) \approx 396.5501 p_u^2 + 0.5997(1 - \cos(q_u)).$$

Despite the change in model, the level set E_π with energy $E(\pi, 0)$ remains the boundary between oscillations and rotations for this nominal pendulum.

We will now simulate the effects of constraining our real acrobot with the VNHC (17), thereby demonstrating that VNHCs are robust to model mismatch. According to Theorem 4, the control parameter I must be "small" for our VNHC to inject (or dissipate) energy into the simplified acrobot. Unfortunately, the Theorem does not specify how small $|I|$ must be; while we could make it arbitrarily small in simulations, we will eventually implement this VNHC on a physical testbed where $|I|$ must be large enough to overcome friction.

Setting $\bar{q}_a = 1$, we experimentally determined that $|I| = 10$ is a viable control parameter, so this is the value we will use for all simulations and experiments. In other words, our *injection VNHC* is (17) with $I = 10$ while our *dissipation VNHC* is (17) with $I = -10$.

A. Energy Injection

In simulation, we stabilized the injection VNHC for the acrobot using the controller (14). We initialized the acrobot on the constraint manifold with initial condition $(q_u, p_u) = (\pi/32, 0)$ and simulated the constrained system for 30 seconds. The resulting orbit is plotted in Figure 5.

The level set E_π with energy $E(\pi, 0)$ is outlined in black. Recall that this level set is the boundary between oscillations and rotations of the nominal pendulum. The points where the orbit exits E_π are marked with black asterisks, with the final

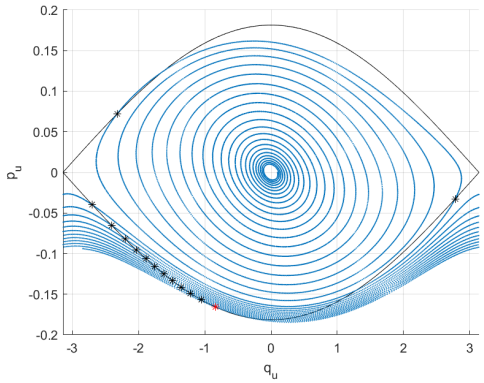

Fig. 5: A simulation of the acrobot gaining energy.

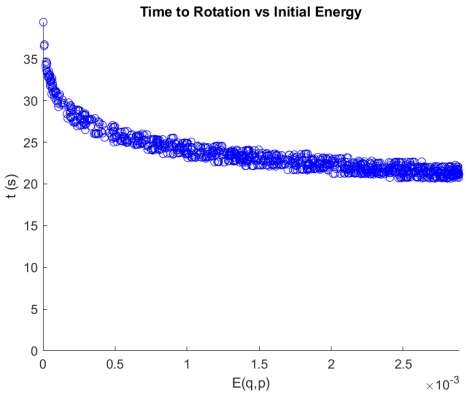

Fig. 6: Monte Carlo simulation for energy injection.

departure marked by a red asterisk. Interestingly, our choice of I is large enough that we observe significant differences between the nominal pendulum and the constrained dynamics: E_π intersects the p_u-axis at $|p_u| \approx 0.17$, yet the constrained acrobot begins rotating once it hits the p_u-axis at $|p_u| \approx 0.16$. This indicates that higher values of I enable the acrobot to gain energy faster and begin rotating sooner, so long as the actuator does not saturate.

To verify numerically that the acrobot would consistently achieve rotations, we ran a Monte-Carlo [22] simulation where we initialized the acrobot randomly inside the sublevel set

$$\left\{(q_u, p_u) \in \mathbb{S}^1 \times \mathbb{R} \mid E(q_u, p_u) \leq E\left(\frac{\pi}{32}, 0\right)\right\},$$

and measured how long it took to begin rotating. The results in Figure 6 show that the acrobot always rotated within 20–40 seconds.

B. Energy Dissipation

In simulation, we stabilized the dissipation VNHC and initialized the acrobot on the constraint manifold with a rotation $(q_u, p_u) = (0, 0.18)$. We simulated the constrained system for 30 seconds and plotted the resulting orbit in Figure 7. As expected, the acrobot slows down over time. We highlight the locations where the orbit crossed the set E_π by black asterisks, with the final crossing in red. After this final crossing, the acrobot ceased rotating and its oscillations decayed to zero.

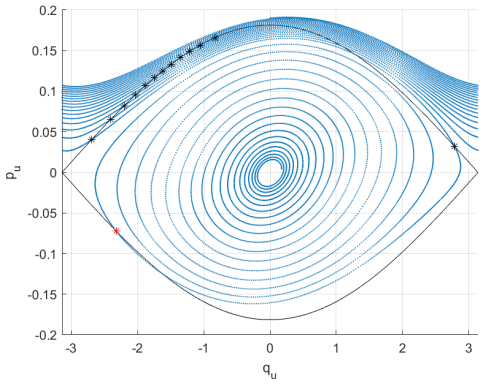

Fig. 7: A simulation of the acrobot dissipating energy.

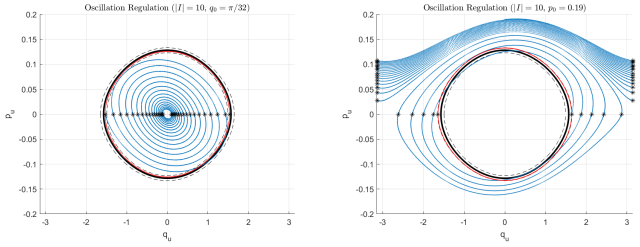

(a) Stabilizing an oscillation from below.

(b) Stabilizing an oscillation from above.

Fig. 8: Using a supervisor to stabilize the oscillation with peak angle $q_{\text{des}} = \pi/2$. The desired oscillation is depicted with a solid black line.

C. Oscillation Regulation

Recall from Section IV-B that one can use a supervisor to stabilize oscillations by appropriately toggling between injection and dissipation VNHCs whenever the orbit of the acrobot crosses the q_u-axis. Figure 8 shows the supervisor stabilizing an oscillation with body angle $q_{\text{des}} = \pi/2$ and a 5% hysteresis, meaning $\delta = 0.05$. The supervisor reevaluated its choice of VNHC at each black asterisk; the red contour corresponds to the part of the orbit where the supervisor kept the leg extended, because the oscillation was within tolerance of q_{des}. The solid black line is the desired oscillation, and the dashed black lines show the hysteresis around that orbit.

In Figure 8a the acrobot was initialized at $(q_u, p_u) = (\pi/32, 0)$; here the supervisor injected energy to stabilize the desired orbit. In Figure 8b the acrobot was initialized at the rotation $(q_u, p_u) = (0, 0.19)$; note that the supervisor is first enabled at the line $|q_u| = \pi$ and dissipates energy. Eventually the acrobot begins a rocking motion and the supervisor is enable again each time the acrobot hits the q_u-axis. The supervisor continues to dissipate energy until it stabilizes the desired oscillation.

D. Rotation Regulation

One can also use a supervisor to stabilize rotations through the mechanism described in Section IV-B, where the supervisor toggles between injection and dissipation VNHCs at each crossing of the p_u-axis. Rotation regulation for the acrobot

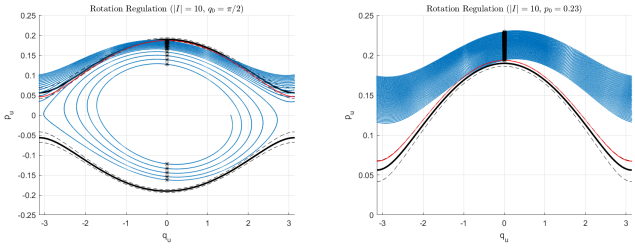

(a) Stabilizing a rotation from below.

(b) Stabilizing a rotation from above.

Fig. 9: Using a supervisor to stabilize the rotation with maximal momentum $p_{\text{des}} = 0.23$. The desired rotation is depicted with a solid black line.

is demonstrated in Figure 9, where the supervisor stabilizes $p_{\text{des}} = 0.19$ with a 2% hysteresis $\delta = 0.02$. The supervisor evaluated its choice of VNHC at each black asterisk. Once it was within range of p_{des} it extended the legs completely, the orbit of which is shown in red.

In Figure 9a the acrobot was initialized at the oscillation $(q_u, p_u) = (\pi/2, 0)$; here the supervisor injected energy until the orbit hit the p_u-axis near p_{des}. In Figure 9b the acrobot was initialized at the (fast) rotation $(q_u, p_u) = (0, 0.23)$; here the supervisor dissipated energy. In both cases, the desired rotation was stabilized correctly.

Note the difference in shape between the blue rotations of the dissipation VNHC and the red rotation of the nominal pendulum in Figure 9: the red one slows down much more near $|q_u| = \pi$. This difference arises because of the size of I: if $|I|$ were smaller, the blue rotations would be more similar in shape to the red one because the constrained dynamics for the dissipation VNHC would be well approximated by the nominal pendulum.

E. Summary of Results

The simulation results in this section demonstrate the energy regulation capabilities of our VNHC. We were able to stabilize both oscillations and rotations by implementing a control supervisor which toggled between injection, dissipation, and leg-extension VNHCs. In particular, these simulations indicate that our VNHC works even for acrobots whose limbs have differing masses and lengths.

VI. Physical Experiments

A. Hardware Description

In this section we will demonstrate that our VNHC is robust to friction, sensor noise, and other real-world considerations by testing it on our physical acrobot (Figure 10). This platform is called SUGAR, which stands for Simple Underactuated Gymnastics and Acrobatics Robot. Its dynamic parameters are outlined in Table I.

SUGAR is comprised of two 3D-printed links: a torso and a leg. The torso houses an Arduino Nano microcontroller unit (MCU) which controls a Dynamixel RX24F servo motor between the torso and the leg. The MCU and the motor are powered by a 12V battery held in a compartment in the leg.

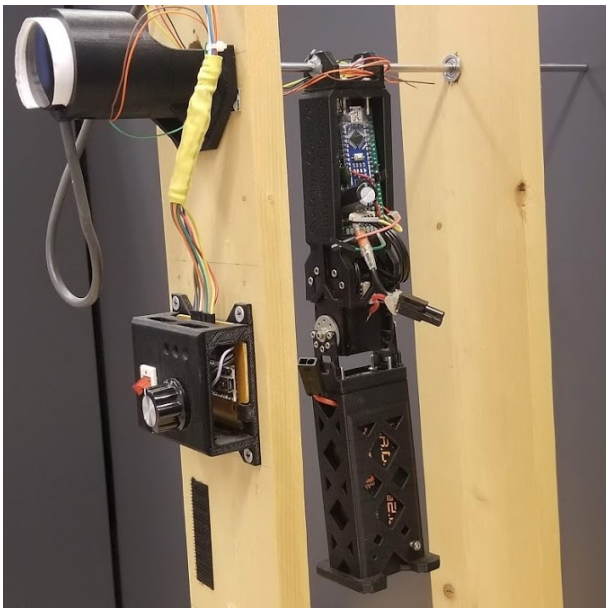

Fig. 10: SUGAR is the physical acrobot built by Wang [4].

The torso is rigidly attached to a metal bar, which is held up by two wooden posts. On the exterior of one post is a control box with a power switch and a second Arduino Nano 328. The purpose of this control box is to read measurements from a rotary encoder connected to the metal bar, and to transmit these measurements to the MCU. The two Arduinos communicate through wires attached to a slip ring on the metal bar, and the signals are transmitted via I2C. The control box also provides a USB interface which allows the user to read the data from the acrobot in real time.

The rotary encoder directly measures q_u, and the Dynamixel servo motor provides measurements of q_a. However, there are no sensors measuring the velocity $\dot{q}$, which means we cannot directly evaluate p_u and p_a. To resolve this issue, the MCU estimates $\dot{q}$ by applying a washout filter to sequential measurements of q. We then compute $p = M(q)\dot{q}$ for use in the VNHC controller.

The communication speed between Arduinos restricts the sampling rate of p to 500Hz. This low sampling rate results in a noisy momentum signal which suffers from noticeable phase lag. This also rate-limits the control signal to 500Hz, which impacts any control implementation.

Finally, the Dynamixel servo motor does not have a torque control mode; instead, we can assign the servo setpoint at iteration $k \in \mathbb{Z}_{>0}$ via $q_a^k = \arctan(Ip_u^{k-1})$. This negatively affects the stabilization to the constraint manifold because we are introducing timing errors from the servo's built-in PID controller.

B. Experimental Results

We performed the following tests on SUGAR with the energy injection VNHC.

1) **Baseline Test:** we initialized SUGAR at $(q_u, p_u) \approx (\pi/8, 0)$. The resulting orbit in Figure 11 shows that SUGAR clearly gaining energy over time. Its motion looks similar to that of the energy injection simulation (Figure 5), though its energy gain ceases once it reaches a rotation with energy $E(0, 0.195)$. The energy gain likely ceases because of friction at the pivot, which was not modelled in simulation.
2) **Perturbation Test 1:** we initialized SUGAR at $(q_u, p_u) \approx (\pi, 0)$, let it run for 15 seconds, then introduced a rod as SUGAR passed through the bottom of its arc. This caused a collision which stopped SUGAR in its tracks, at which point we immediately removed the rod so SUGAR could continue unperturbed. The resulting orbit is shown in Figure 12. The blue rotation curve corresponds to the orbit before the disturbance, while the red spiral confirms that SUGAR begins oscillating after it was stopped. After the collision, SUGAR gains energy and eventually starts rotating again.
3) **Perturbation Test 2:** to see how SUGAR would respond when pushed, we allowed it to rotate unperturbed for 15 seconds and then pushed it in its direction of motion. The orbit in Figure 13a shows that SUGAR, when pushed, rotates with energy $E(0, -0.22)$, but then slows down until it reaches a rotation with energy $E(0, -0.195)$. We repeated this test by pushing SUGAR against its direction of motion. The orbit in Figure 13b demonstrates that SUGAR readily changes direction,

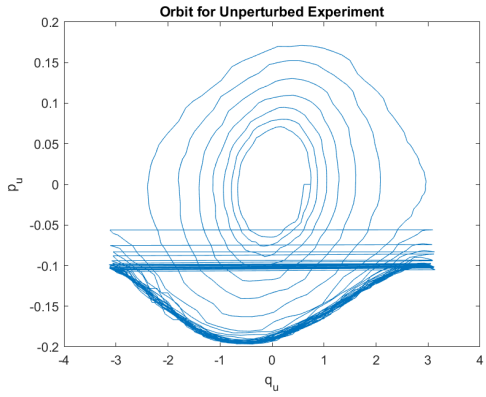

Fig. 11: Baseline Test: SUGAR's baseline energy injection orbit.

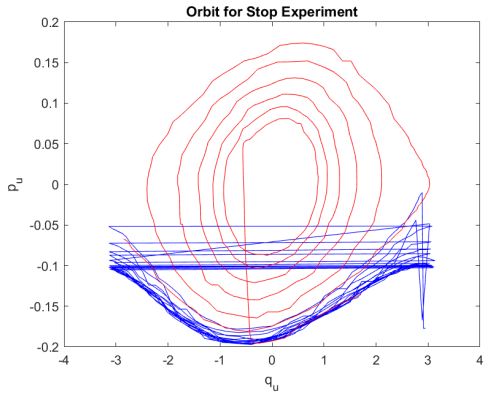

Fig. 12: Perturbation Test 1: SUGAR's orbit before (blue) and after (red) stopping.

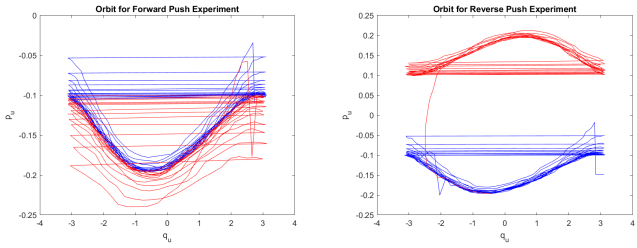

(a) The forwards push test. (b) The reverse push test.

Fig. 13: Perturbation Test 2: SUGAR's orbit before (blue) and after (red) pushing.

and quickly achieves its maximum speed with energy $E(0, 0.195)$.

In simulation, the acrobot was able to gain energy even when initialized with energy $E(q_u, p_u) > E(0, 0.195)$. The baseline and push tests suggest that our VNHC injects energy into SUGAR only on $\mathcal{O}_2(0.195)$. This difference between simulation and implementation is likely due to friction, as well as timing errors incurred by the PID controller in the servo motor.

C. Summary of Results

We performed three tests on SUGAR: a baseline energy injection test, a stop test, and a push test. These experiments demonstrate that VNHC-based energy injection is robust to significant model mismatch, friction, sensor noise, discretized control implementation, rate-limited measurement and control signals, and dramatic external disturbances.

VII. Proof of Theorem 4

In this section we prove Theorem 4, which claims the acrobot constrained by the VNHC (17) will gain or lose energy on $\mathcal{O}_1$ and $\mathcal{O}_2(\rho)$ for "small enough" values of I.

Here is intuition behind this proof: for each of $\mathcal{O}_1$ and $\mathcal{O}_2(\rho)$, we can find a diffeomorphism from (q_u, p_u) into pseudo-polar coordinates (r, θ) adapted to level sets of $E(q_u, p_u)$; that is, when $I = 0$ in (17), the pseudo-radius r chooses a level set of E and the pseudo-angle θ chooses a point on that level set. We will show that $r(t)$ increases "on average", which implies E also increases "on average", and that the original constrained dynamics (18) are gaining energy on the domain of the diffeomorphism.

The following lemma provides a set of conditions on the (r, θ)-dynamics under which energy will increase on a domain $D \subset \mathbb{S}^1 \times \mathbb{R}$; later in this section, we will assign $D \subset \mathcal{O}_1$ or $D \subset \mathcal{O}_2(\rho)$ and apply this lemma to prove the claims in Theorem 4.

Lemma 2: Consider the simplified acrobot (6) constrained by the VNHC (17), whose constrained dynamics are (18). Let $D \subset \mathbb{S}^1 \times \mathbb{R}$ be open and let $]\underline{r}, \overline{r}[\subset \mathbb{R}_{>0}$. Suppose there exists a diffeomorphism

$$T : D \to]\underline{r}, \overline{r}[\times \mathbb{S}^1$$
$$(q_u, p_u) \mapsto (r, \theta),$$

yielding the new constrained dynamics $\dot{r} = f_r(\theta, r, I)$, $\dot{\theta} = f_\theta(\theta, r, I)$. Suppose that $f_r(\theta, r, 0) \equiv 0$ and $f_\theta(\theta, r, 0) > 0$. Let $g(\theta, r, I) := f_r(\theta, r, I)/f_\theta(\theta, r, I)$, and assume that $(\partial g/\partial r)(\theta, r, 0) \equiv 0$. Assume also that $b(\theta, r) := (\partial g/\partial I)(\theta, r, 0)$ is 2π-periodic in θ, and that there exists $\epsilon > 0$ such that $S(r_0) := \int_0^{2\pi} b(\sigma, r_0) d\sigma \geq \epsilon$ for all $r_0 \in]\underline{r}, \overline{r}[$. Then there exists $I^\star > 0$ small enough that the constrained dynamics gain energy on D for all $I \in]0, I^\star]$, and lose energy on D for all $I \in [-I^\star, 0[$.

Proof: Since $f_\theta(\theta, r, 0) > 0$ and f_θ is continuous in I, there exists $I_1 > 0$ small enough that $\dot{\theta} > 0$ for all $I \in [-I_1, I_1]$. Hence, we can perform a time reparameterization $t = t(\theta)$ to get a time-scaled pseudo-radius $\hat{r}(\theta) := r(t(\theta))$. This reduces the system $(\dot{r}, \dot{\theta})$ into the scalar time-varying ODE

$$\begin{cases} \hat{r}' = \frac{dr}{dt}\frac{dt}{d\theta}\big|_{r=\hat{r}} = g(\theta, \hat{r}, I), \\ \hat{r}(0) = r_0, \end{cases} \tag{23}$$

with state $\hat{r}$, where now θ represents time, prime denotes differentiation by θ, and $r_0 \in]\underline{r}, \overline{r}[$ is the initial condition.

Let $\hat{r}(\theta, r_0, I)$ be the solution to (23). Taking the Taylor expansion of this solution around $I = 0$ yields $\hat{r}(\theta, r_0, I) = \hat{r}(\theta, r_0, 0) + I\hat{r}_1(\theta, r_0) + R(\theta, r_0, I)$. Here, $\hat{r}(\theta, r_0, 0) \equiv r_0$ because $g(\theta, \hat{r}, 0) \equiv 0$, the function $\hat{r}_1(\theta, r_0)$ is the solution to the linear time-varying ODE

$$\begin{cases} \hat{r}_1' = \frac{\partial g}{\partial \hat{r}}(\theta, r_0, 0)\hat{r}_1 + b(\theta, r_0), \\ \hat{r}_1(0) = 0, \end{cases} \tag{24}$$

and the remainder term $R(\theta, r_0, I)$ is $O(I^2)$.

Since $(\partial g/\partial \hat{r})(\theta, r_0, 0) \equiv 0$, the solution of (24) can be obtained by quadrature, giving $\hat{r}_1(\theta, r_0) = \int_0^\theta b(\sigma, r_0) d\sigma$. Recall that $b(\theta, r_0)$ is 2π-periodic in θ, so there is a well-defined Poincaré map describing how $\hat{r}$ changes each time θ increases by 2π. This map is

$$P :]\underline{r}, \overline{r}[\to \mathbb{R}_{\geq 0} \tag{25}$$
$$r_0 \mapsto \hat{r}(2\pi, r_0, I),$$

which expands to $P(r_0) = r_0 + IS(r_0) + R(2\pi, r_0, I)$. In other words, we can understand the evolution of $\hat{r}$ by studying the dynamics of the discrete-time system

$$r_{n+1} = P(r_n) = r_n + IS(r_n) + R(2\pi, r_n, I), \tag{26}$$

with initial condition r_0.

If $r_{n+1} \in]\underline{r}, \overline{r}[$, the orbit $(q_u(t), p_u(t))$ starting at $T^{-1}(r_n, 0)$ remained in D as θ increased by 2π and landed at $T^{-1}(r_{n+1}, 2\pi)$; otherwise, this orbit exited D before θ reached 2π. Hence, proving the constrained dynamics gain energy on D is equivalent to finding $N \in \mathbb{Z}_{>0}$ such that $r_n \geq \overline{r}$ for all $n \geq N$. Using a perturbation analysis (see Khalil [23, Theorem 10.1]), we know there exists some $I_2 \in]0, I_1]$ and $\kappa > 0$ such that $|R(\theta, r, I)| \leq \kappa I^2$ for all $\theta \in [0, 2\pi]$, $r \in]\underline{r}, \overline{r}[$, and $I \in [-I_2, I_2]$. Taking this fact alongside the assumption that $S(r_0) \geq \epsilon$, we find a lower bound $r_{n+1} \geq r_n + I\epsilon - \kappa I^2$. Let $0 < I^\star < \min\{I_2, \epsilon/\kappa\}$. Then for each $I \in]0, I^\star]$, the value $\gamma := I\epsilon - \kappa I^2$ is strictly positive, so $P(r_0) \geq r_0 + \gamma$. Therefore, $r_n \geq r_0 + n\gamma$, and all solutions of (26) eventually flow past $\overline{r}$.

We conclude that, for $I \in]0, I^\star]$, the constrained dynamics gain energy on D. Changing the sign of I changes the direction of the above inequalites, so that $r_n \leq r_0 - n\gamma$. In this case all orbits of (26) flow below $\underline{r}$, i.e., the constrained dynamics lose energy on D. ■

A. Energy Gain on $\mathcal{O}_1$

To prove the first part of Theorem 4, we apply [24, Eqn. (9)] to find pseudo-polar coordinates adapted to level sets of E on $\mathcal{O}_1 \backslash \{(0,0)\}$. The resulting coordinate transformation is

$$r = \arccos\left(\cos(q_u) - \frac{p_u^2}{30m^2gl^3}\right), \tag{27}$$

$$\theta = \arctan_2\left(-\operatorname{sgn}(p_u)\sqrt{1-\frac{q_u^2}{r^2}}, \frac{q_u}{r}\right)\Bigg|_{r=r(q_u,p_u)}, \tag{28}$$

where $(r,\theta) \in]0,\pi[\times\mathbb{S}^1$. One can verify that the inverse to this transformation is

$$q_u = rc_\theta,$$
$$p_u = -\operatorname{sgn}(s_\theta)\sqrt{30m^2gl^3\cos(rc_\theta - c_r)},$$

where for shorthand we write $c_\theta := \cos(\theta)$, $s_\theta := \sin(\theta)$, $c_r := \cos(r)$, and $s_r := \sin(r)$. We now verify these pseudo-polar coordinates satisfy the requirements of Lemma 2. Note: we omit the expressions for $f_r(\theta, r, I)$ and $f_\theta(\theta, r, I)$ as they are too long for print.

It is straightforward to show that $f_r(\theta, r, 0) \equiv 0$ and

$$f_\theta(\theta, r, 0) = \sqrt{\frac{6g}{5l}}\sqrt{\frac{\cos(rc_\theta) - c_r}{r^2 s_\theta^2}}. \tag{29}$$

Observe that (29) has removable singularities at $\theta \in \{0, \pi\}$. Taking the limit as θ approaches these points yields

$$\lim_{\theta\to 0} f_\theta(\theta, r, 0) = \lim_{\theta\to\pi} f_\theta(\theta, r, 0) = \sqrt{\frac{6gs_r}{10lr}}, \tag{30}$$

which is smooth and well-defined for all $r \in]0,\pi[$. From (29)–(30), one can verify that $f_\theta(\theta, r, 0) > 0$ as required. Defining $g(\theta, r, I)$ as in Lemma 2, one can also verify that $(\partial g/\partial r)(\theta, r, 0) \equiv 0$.

Symbolic computations reveal that $b(\theta, r_0) = Ka(\theta, r_0)$, where

$$K := \frac{\bar{q}_a\sqrt{30m^2gl^3}}{15},$$
$$a(\theta, r_0) := \frac{r_0|s_\theta|\left(5c_{r_0}\cos(r_0c_\theta) - 8\cos(r_0c_\theta)^2 + 3\right)}{s_{r_0}\sqrt{\cos(r_0c_\theta) - c_{r_0}}}.$$

Notice that K is a positive constant which depends only on m, g, l, and $\bar{q}_a$, while $a(\theta, r_0)$ is adimensional and 2π-periodic in θ. This means the integral of $a(\theta, r_0)$ can be computed once for all acrobots; hence, there exists $\epsilon > 0$ such that $S(r_0) := \int_0^{2\pi} b(\sigma, r_0)d\sigma \geq \epsilon$ if and only if there exists $\delta > 0$ such that $Q(r_0) := \int_0^{2\pi} a(\sigma, r_0)d\sigma \geq \delta$ for every $r_0 \in]0,\pi[$.

Unfortunately, this latter statement is not true. The plot of $Q(r_0)$ for $r_0 \in [10^{-10}, \pi - 10^{-3}]$ is shown in Figure 14. We see that it is strictly positive and monotonically increasing, with an asymptote at $r_0 = \pi$, but $Q(r_0) \to 0$ as $r_0 \to 0$.

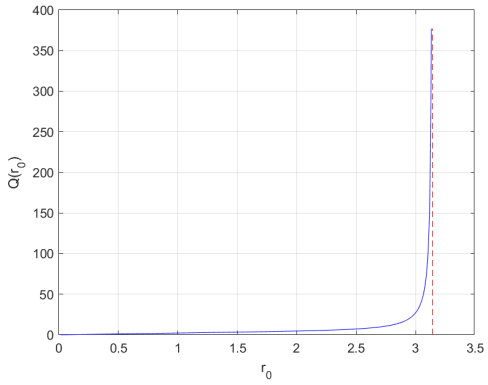

Fig. 14: The plot of $Q(r_0)$.

Thankfully, we can still use Lemma 2 on an appropriate subset of $\mathcal{O}_1$. To find this subset, first recall the discrete-time pseudo-radius dynamics (26) from the proof of Lemma 2. Linearizing (26) at $r_0 = 0$ yields

$$P'(0) = 1 + IKQ'(0) + R'(2\pi, 0, I),$$

where the prime now denotes differentiation with respect to r. One can show that

$$Q'(0) = \int_0^\pi \lim_{r_0\to 0^+}\frac{\partial a}{\partial r}(\sigma, r_0)d\sigma = \frac{\pi}{2\sqrt{2}} > 0.$$

Since $R(2\pi, 0, I)$ is $O(I^2)$, so is $R'(2\pi, 0, I)$. Hence, it can be written in the form $R'(2\pi, 0, I) = I^2\tilde{R}(I)$ where $\tilde{R}(I)$ is smooth, bounded, and zero at $I = 0$. Thus, there exists $I_0 > 0$ such that $IKQ'(0) + I^2\tilde{R}(I) > 0$ for all $I \in]0, I_0]$, which implies $P'(0) > 1$ for all $I \in]0, I_0]$. This means the origin is a repeller, so there exists some (unknown) $\mu > 0$ where $]0, \mu]$ is negatively invariant for (26), and all solutions in this interval flow through $r = \mu$. If $I < 0$, we have $P'(0) < 1$ and the origin is an asymptotically stable equilibrium for (26).

Let $E_{\leq\mu}$ be the sublevel set of the energy $E(\mu, 0)$. Since there exists $\delta_\mu > 0$ such that $Q(r_0) \geq \delta_\mu$ for $r_0 \in [\mu, \pi[$, all conditions of Lemma 2 are valid on the annulus $D_\mu = \mathcal{O}_1 \backslash E_{\leq\mu}$. Hence, there exists some $I_1(\mu) > 0$ such that the acrobot gains/loses energy everywhere on D_μ. Taking $I^\star = \min\{I_0, I_1(\mu)\}$, the acrobot will gain energy on $\mathcal{O}_1$ for $I \in]0, I^\star]$ and lose energy for $I \in [-I^\star, 0[$.

B. All Acrobots Rotate

We have proven that any acrobot constrained by our VNHC (17) will gain (or lose) energy on $\mathcal{O}_1$. We must now prove that every acrobot will begin rotating, i.e., that when $I \in]0, I^\star]$ almost every orbit initialized in $\mathcal{O}_1$ will reach the line $|q_u| = \pi$.

The definition of energy gain only guarantees that orbits initialized in $\mathcal{O}_1$ will escape compact subsets of $\mathcal{O}_1$ in finite time. For an orbit of the acrobot to reach the line $|q_u| = \pi$, it must first escape the closure $\bar{\mathcal{O}}_1 = \mathcal{O}_1 \cup E_\pi$ through its boundary, the level set E_π with energy level $E(\pi, 0)$.

Taking the Jacobian of the constrained dynamics (18) at the upright equilibrium $(q_u, p_u) = (\pi, 0)$ yields

$$J = \begin{bmatrix} -\frac{6mgl\bar{q}_a I}{5} & \frac{1-2m^2gl^3\bar{q}_a^2 I^2}{5ml^2} \\ 3mgl & mgl\bar{q}_a I \end{bmatrix},$$

which has characteristic polynomial

$$\det(\lambda I_2 - J) = \lambda^2 + \frac{mgl\bar{q}_a I}{5}\lambda - 3g.$$

This polynomial always has exactly one root with positive real part. The equilibrium $(\pi, 0)$ is therefore unstable, so the stable manifold Π^+ of initial conditions converging to $(\pi, 0)$ is one-dimensional, and hence is of measure zero in $\mathbb{S}^1 \times \mathbb{R}$.

Using $x(t) := (q_u(t), p_u(t))$ as shorthand, let $x(0) \in \mathcal{O}_1$ be a nonzero initial condition of the acrobot. Suppose by way of contradiction that the orbit $x(\mathbb{R})$ is confined within $\bar{\mathcal{O}}_1$, and does not exit through E_π into the rotation zone. Since the acrobot gains energy on $\mathcal{O}_1$ and $\bar{\mathcal{O}}_1$ is compact, the Birkhoff Theorem [25] implies that the solution $x(t)$ asymptotically tends to the positive limit set, which is the largest invariant subset of E_π. Taking the limit as $r \to \pi$ of (29)–(30), we get $\dot{\theta} \geq 0$ on E_π with equality if and only if $\theta \in \{0, \pi\}$. Thus, the largest invariant subset of E_π is either the upright equilibrium $\{(\pi, 0)\}$ or E_π itself.

Taking the derivative of $E(q_u, p_u)$ at the p_u-axis yields $\dot{E}(0, p_u) = g/(5l)\sin(q_a)p_u$. This is non-zero on E_π, so E_π is not invariant and the positive limit set of $x(t)$ must be the set $\{(\pi, 0)\}$. Hence, $x(t)$ converges to $(\pi, 0)$, so $x(0) \in \Pi^+$. Since Π^+ is a set of measure zero in $\mathbb{S}^1 \times \mathbb{R}$, almost every orbit initialized in $\mathcal{O}_1$ must escape at least once through E_π into the rotation domain.

Using this fact, we now prove that almost every orbit in $\mathcal{O}_1$ will cross the line $|q_u| = \pi$. Let $x(0) \in \mathcal{O}_1$ and suppose that the orbit $x(t)$ does not hit the line $|q_u| = \pi$. We claim that this orbit must remain in the compact set $\mathbb{S}^1 \times [-K, K]$, for some $K > 0$. Suppose otherwise; then for arbitrary $K > 0$, there exists some $t_K > 0$ such that $|p_u(t_K)| = K$. From (18), we see that $-3mgl \leq \dot{p}_u \leq 3mgl$ and $\dot{q}_u \geq c_1 p_u - c_2$ for some constants $c_1, c_2 > 0$. This implies there exists a $t_{1/2} > 0$ (independent of K) where $|p_u(t)| >= K/2$ and $|\dot{q}_u(t)| \geq c_1 K/2 - c_2$ for $t \in [t_K, t_K + t_{1/2}]$. Picking K large enough guarantees $q_u(t)$ covers a distance of 2π over this time interval, so the orbit would hit the line $|q_u| = \pi$.

We now know that if $x(t)$ does not hit the line $|q_u| = \pi$, it must remain within the compact set $\mathbb{S}^1 \times [-K, K]$. By the Birkhoff theorem, $x(t)$ approaches a positive limit set L^+, which is either the upright equilibrium $\{(\pi, 0)\}$, or a closed orbit (not fully contained in $\mathcal{O}_1$) which crosses the positive q_u-axis at some point $\bar{q} < \pi$. Suppose L^+ is the latter. Since $]0, \mu]$ is negatively invariant for (26), we must have $\bar{q} > \mu$. The Poincaré map (25) is smooth on $]0, \pi[$, and its image contains $\bar{q}$, so $P^{-1}(\bar{q}) \neq \emptyset$. Take $q' \in P^{-1}(\bar{q})$. If $q' \in]0, \mu]$, then $q' < \bar{q}$; if $q' > \mu$, then we know from the proof of Lemma 2 that $P(q') = \bar{q} \geq q' + \gamma$ for some $\gamma > 0$, so $q' \leq \bar{q} - \gamma < \bar{q}$. In either case, $q' < \bar{q}$, so the orbit starting at q' stays within $\mathcal{O}_1$ and intersects the closed orbit at $\bar{q}$. This violates uniqueness of solutions for the constrained dynamics, so L^+ must be $\{(\pi, 0)\}$, which in turn implies that $x(0) \in \Pi^+$.

We conclude that almost all orbits beginning in $\mathcal{O}_1$ will escape the closure of $\mathcal{O}_1$ and begin rotating by crossing the vertical line $|q_u| = \pi$.

C. Energy Gain on $\mathcal{O}_2(\rho)$

Since $\mathcal{O}_2(\rho) = \bar{\mathcal{O}}_1 \cup \mathcal{R}(\rho)$ (where $\mathcal{R}(\rho)$ is the rotation domain defined in (21)), and since all orbits in $\mathcal{O}_1$ will begin rotating, we need simply prove energy gain on $\mathcal{R}(\rho)$ to prove energy gain on $\mathcal{O}_2(\rho)$. We separate $\mathcal{R}(\rho)$ into its two separate connected components: $\mathcal{R}^+(\rho)$, the set of rotations with $p_u > 0$; and $\mathcal{R}^-(\rho)$, the set of rotations with $p_u < 0$. We take the domain of interest for Lemma 2 to be either of these rotation sets.

We now apply [24, Eqn. (8)] to find pseudo-polar coordinates adapted to rotations. These coordinates are

$$r = \sqrt{p_u^2 + 30m^2gl^3(1 - c_u)}, \tag{31}$$
$$\theta = \operatorname{sgn}(p_u)\, q_u \tag{32}$$

with $]\underline{r}, \overline{r}[=]\sqrt{60m^2gl^3}, \rho[$. The inverse transformation is

$$q_u = \pm\theta,$$
$$p_u = \pm\sqrt{r^2 - 30m^2gl^3(1 - c_\theta)},$$

where the $\pm$ is $+1$ on $\mathcal{R}^+(\rho)$, or -1 on $\mathcal{R}^-(\rho)$.

After computing the constrained dynamics in (r, θ) coordinates, one can verify that $f_r(\theta, r, 0) \equiv 0$ and

$$f_\theta(\theta, r, 0) = \frac{1}{5ml^2}\sqrt{r^2 - 30m^2gl^3(1 - c_\theta)},$$

which is strictly positive as required. Symbolic computations also confirm that $(\partial g/\partial r)(\theta, r, 0) \equiv 0$. The function $b(\theta, r_0) = (\partial g/\partial I)(\theta, r_0, 0)$ is given in the statement of Theorem 4, and by assumption we have $S(r_0) \geq \epsilon$.

Thus, all requirements of Lemma 2 are satisfied, so there exists $I_2(\rho) > 0$ where the acrobot gains energy for $I \in]0, I_2(\rho)]$ (on both $\mathcal{R}^+(\rho)$ and $\mathcal{R}^-(\rho)$). Let $I^\star$ be the value we found for $\mathcal{O}_1$ in Section VII-A, and let $I^{\star\star} = \min\{I^\star, I_2(\rho)\}$. Then the acrobot gains energy on $\mathcal{O}_2(\rho)$ for $I \in]0, I^{\star\star}]$, and dissipates energy for $I \in [-I^{\star\star}, 0[$.

This completes the proof of Theorem 4.

VIII. Conclusion

In this article we applied the framework of virtual nonholonomic constraints to the acrobot, and designed a constraint which emulates giant motion from gymnastics. We proved this constraint will inject energy into the simplified acrobot whose limbs are massless rods of equal length, with equal masses at the tips. We then performed simulations and physical experiments on a real acrobot robot. These demonstrated that virtual nonholonomic constraints are capable of injecting and dissipating energy in a robust manner, while producing realistic biologically-inspired motion.

REFERENCES

[1] P. E. Pidcoe, "The biomechanics principles behind training giant swings," Online, Virginia Commonwealth University, Richmond, VA, USA, August 2005, accessed 11 September 2020. https://usagym.org/pages/home/publications/technique/2005/8/giant.pdf.

[2] V. Sevrez, E. Berton, G. Rao, and R. J. Bootsma, "Regulation of pendulum length as a control mechanism in performing the backward giant circle in gymnastics," *Human Movement Science*, vol. 28, no. 2, pp. 250 – 262, March 2009.

[3] J. Hauser and R. Murray, "Nonlinear controllers for non-integrable systems: the acrobot example," in *1990 American Control Conference*. San Diego, USA: IEEE, May 1990.

[4] X. Wang, "Motion control of a gymnastics robot using virtual holonomic constraints," Master's thesis, University of Toronto, 2016.

[5] E. Papadopoulos and G. Papadopoulos, "A novel energy pumping strategy for robotic swinging," in *2009 17th Mediterranean Conference on Control and Automation*. Thessaloniki, Greece: IEEE, June 2009.

[6] T. Henmi, M. Chujo, Y. Ohta, and M. Deng, "Reproduction of swing-up and giant swing motion of acrobot based on a technique of the horizontal bar gymnast," in *Proceedings of the 11th World Congress on Intelligent Control and Automation*. Shenyang, China: IEEE, June 2014.

[7] X. Zhang, H. Cheng, Y. Zhao, and B. Gao, "The dynamical servo control problem for the acrobot based on virtual constraints approach," in *The 2009 IEEE/RSJ International Conference on Intelligent Robots and Systems*. St. Louis, USA: IEEE, October 2009.

[8] K. Ono, K. Yamamoto, and A. Imadu, "Control of giant swing motion of a two-link horizontal bar gymnastic robot," *Advanced Robotics*, vol. 15, no. 4, pp. 449 – 465, 2001.

[9] J. Horn, A. Mohammadi, K. Hamed, and R. Gregg, "Hybrid zero dynamics of bipedal robots under nonholonomic virtual constraints," *IEEE Control Systems Letters*, vol. 3, no. 2, pp. 386 – 391, April 2019.

[10] T. Takubo, H. Arai, and K. Tanie, "Virtual nonholonomic constraint for human-robot cooperation in 3-d space," in *2000 IEEE/RSJ International Conference on Intelligent Robots and Systems*. Takamatsu, Japan: IEEE, October 2000.

[11] S. Shibata and T. Murakami, "Psd based virtual nonholonomic constraint for human interaction of redundant manipulator," in *Proceedings of the 2004 IEEE International Conference on Control Applications*. Taipei,Taiwan: IEEE, September 2004.

[12] J. D. Castro-Díaz, P. Sánchez-Sánchez, A. Gutiérrez-Giles, M. Arteaga-Pérez, and J. Pliego-Jiménez, "Experimental results for haptic interaction with virtual holonomic and nonholonomic constraints," *IEEE Access*, vol. 8, pp. 120 959 – 120 973, July 2020.

[13] S. Vozar, Z. Chen, P. Kazanzides, and L. L. Whitcomb, "Preliminary study of virtual nonholonomic constraints for time-delayed teleoperation," in *2015 IEEE/RSJ International Conference on Intelligent Robots and Systems*. Hamburg, Germany: IEEE, October 2015.

[14] B. Griffin and J. Grizzle, "Nonholonomic virtual constraints for dynamic walking," in *2015 54th IEEE Conference on Decision and Control*. Osaka, Japan: IEEE, December 2015.

[15] W. K. Chan, Y. Gu, and B. Yao, "Optimization of output functions with nonholonomic virtual constraints in underactauted bipedal walking control," in *2018 Annual American Control Conference*. Milwaukee, USA: IEEE, June 2018.

[16] J. C. Horn, A. Mohammadi, K. A. Hamed, and R. D. Gregg, "Nonholonomic virtual constraint design for variable-incline bipedal robotic walking," *IEEE Robotics and Automation Letters*, vol. 5, pp. 3691 – 3698, February 2020.

[17] R. D. Schafer, *An Introduction to Non-Associative Algebras*. New York: Dover Publications, 1996.

[18] L. D. Landau and E. M. Lifschitz, *Mechanics*, 3rd ed. Butterworth-Heinemann, January 1982.

[19] G. Golub and W. Kahan, "Calculating the singular values and pseudo-inverse of a matrix," *Journal of the Society for Industrial and Applied Mathematics: Series B, Numerical Analysis*, vol. 2, no. 2, pp. 204–224, 1965.

[20] M. Maggiore and L. Consolini, "Virtual holonomic constraints for euler-lagrange systems," *IEEE Transactions on Automatic Control*, vol. 58, no. 4, pp. 1001 – 1008, April 2013.

[21] S. Wirkus, R. Rand, and A. Ruina, "How to pump a swing," *The College Mathematics Journal*, vol. 29, no. 4, pp. 266 – 275, 1998.

[22] N. Metropolis, "The beginning of the monte carlo method," *Los Alamos Science*, pp. 125–130, 1987, 1987 special issue dedicated to Stanislaw Ulam.

[23] H. K. Khalil, *Nonlinear Systems*, 3rd ed. Upper Saddle River, NJ 07485: Prentice Hall, 2002.

[24] A. Mohammadi, M. Maggiore, and L. Consolini, "Dynamic virtual holonomic constraints for stabilization of closed orbits in underactuated mechanical systems," *Automatica*, vol. 94, pp. 112 – 124, August 2018.

[25] G. D. Birkhoff, *Dynamical Systems*. Colloquium Publications, 1927, vol. 9.